

# The Phase Diagram of the Quark-Meson Model

B.-J. Schaefer<sup>a</sup> and J. Wambach<sup>a,b</sup>

<sup>a</sup>Institut für Kernphysik, TU Darmstadt, D-64289 Darmstadt, Germany

<sup>b</sup>Gesellschaft für Schwerionenforschung GSI, D-64291 Darmstadt, Germany

October 24, 2018

PACS:

## Abstract

Within the proper-time renormalization group approach, the chiral phase diagram of a two-flavor quark-meson model is studied. In the chiral limit, the location of the tricritical point which is linked to a Gaussian fixed point, is determined. For quark chemical potentials smaller than the tricritical one the second-order phase transition belongs to the  $O(4)$  universality class. For temperatures below the tricritical one we find initially a weak first-order phase transition which is commonly seen in model studies and also in recent lattice simulations. In addition, below temperatures of  $T \lesssim 17$  MeV we find two phase transitions. The chiral restoration transition is initially also of first-order but turns into a second-order transition again. This leads to the possibility that there may be a "second tricritical" point in the QCD phase diagram in the chiral limit.

# 1 Introduction

Recently, the phase diagram of the chiral phase transition has received renewed interest with the emergence of improved lattice techniques at finite quark chemical potential,  $\mu$ . Through heavy-ion collision experiments at RHIC, the LHC and the future GSI facility parts of the phase diagram may be accessible. As one of the prominent features of the QCD phase diagram, the existence of a (tri-)critical endpoint of a first-order phase transition line has emerged. This is strongly suggested by model calculations and also indicated by lattice simulations. The precise location of this point is still unknown. In the chiral limit, the critical endpoint becomes a tricritical one corresponding to a Gaussian fixed point. In this limit, the chiral finite-temperature transition at vanishing  $\mu$  is likely to be of second-order for two-flavor QCD, where the critical transition line is expected to fall into the  $O(4)$ -universality class in three dimensions [1]. For finite current masses, the  $O(4)$ -transition line converts to a smooth crossover and the tricritical point turns into a fixed point belonging to the  $3d$  Ising universality class [2, 3, 4].

Second-order phase transitions are characterized by long-wavelength fluctuations of the order parameter. Thus, the critical and non-critical regions of the phase diagram, including first-order phase transitions, can best be described by renormalization group (RG) methods. We employ an analytical RG approach, the proper-time renormalization group (PTRG) [5, 6, 7], to investigate the QCD phase diagram for two quark flavors. As a result of integrating the quantum and thermal fluctuations with a certain cutoff scale  $k$ , we obtain a flow equation for the scale-dependent action. Following the scale evolution towards  $k = 0$ , we arrive at the effective action which contains all thermodynamically relevant universal and non-universal information.

The paper is organized as follow: In the Sec. 2 we derive the analytical PTRG flow equation for an optimized smearing function. This allows to find analytical threshold functions for finite temperatures and chemical potentials. In this way, the numerical summation of Matsubara terms can be circumvented and the numerical error especially for small temperatures during the evolution is reduced. In Sec. 2.1 we consider analytical limits of the full flow equation in order to elucidate its intuitive structure and sketch the numerical implementation in Sec. 2.2. The resulting phase diagram for massless quarks is presented and explored in some detail in Sec. 3. Finally, we summarize and conclude in Sec. 4.

## 2 The flow equations for finite $T$ and $\mu$

As an effective realization of two-flavor QCD, we use the effective action of a linear quark-meson model defined at a scale  $\Lambda$  in the ultraviolet (UV) region of the theory in four Euclidean dimensions by<sup>1</sup>

$$\Gamma_\Lambda[\Phi] = \int d^4x \left\{ \bar{q}[\gamma^\mu \partial_\mu + g(\sigma + i\vec{\tau}\vec{\pi}\gamma_5)]q + \frac{1}{2}(\partial_\mu\sigma)^2 + \frac{1}{2}(\partial_\mu\vec{\pi})^2 + V_\Lambda(\sigma^2 + \vec{\pi}^2) \right\} \quad (1)$$

with one isoscalar-scalar  $\sigma$ -meson and three isovector-pseudoscalar pions  $\vec{\pi}$ . The fermionic fields  $q(x)$  and  $\bar{q}(x)$  incorporate  $N_f = 2$  flavor and  $N_c = 3$  color degrees of freedom.  $\vec{\tau}$  labels the three Pauli matrices. The Yukawa coupling  $g$  is kept constant during the RG evolution. The purely mesonic general effective potential term  $V_\Lambda$  is a function of the  $O(4)$ -symmetric field  $\vec{\phi}^2 = \sigma^2 + \vec{\pi}^2$ . As initial condition in the UV we choose for  $V_\Lambda$  the truncation

$$V_\Lambda(\sigma^2 + \vec{\pi}^2) = \frac{m_\Lambda^2}{2}(\sigma^2 + \vec{\pi}^2) + \frac{\lambda_\Lambda}{4}(\sigma^2 + \vec{\pi}^2)^2 \quad (2)$$

with the parameters  $m_\Lambda^2$  and  $\lambda_\Lambda$  to be specified later. The wavefunction renormalizations for the meson- and quark fields are neglected in this approximation.

The coarse-grained, infrared-finite and renormalization-group improved flow equation for the scale dependent effective action  $\Gamma_k[\Phi]$  of a given theory is governed by

$$\partial_t \Gamma_k[\Phi] = -\frac{1}{2} \int_0^\infty \frac{d\tau}{\tau} [\partial_t f_k(\tau k^2)] \text{Tr} \exp\left(-\tau \Gamma_k^{(2)}[\Phi]\right), \quad (3)$$

where  $\text{Tr}$  denotes a four-dimensional momentum integration and a trace over all given inner spaces (e.g. Dirac, color and/or flavor-space). Details concerning the derivation of this flow equation and inherent approximations can be found in Refs. [5, 8].  $\Gamma_k^{(2)}[\Phi]$  represents the full inverse propagator and is given by a second functional derivative of  $\Gamma_k$  with respect to the appropriate field components

$$\Gamma_k^{(2)}[\Phi] = \frac{\delta^2 \Gamma_k[\Phi]}{\delta \Phi \delta \Phi} \quad (4)$$

---

<sup>1</sup>The argument  $\Phi$  of the effective action is a short-hand notation of all incorporated fields.

If one replaces the effective action derivative  $\Gamma^{(2)}$  on the right-hand side of Eq. (3) by the corresponding classical action  $S^{(2)}$  one obtains the one-loop effective action [5, 7]. The replacement of the classical action  $S^{(2)}$  by the scale-dependent effective action on the right-hand side of Eq. (3) is called RG improvement.

By means of a Schwinger proper-time regularization, an infrared-finite renormalization group equation (PTRG) is obtained. The infrared (IR) scale is given by  $t = \ln(k/\Lambda)$  where  $\Lambda$  denotes the high momentum (UV) scale. One important ingredient of the flow equation (3) is the *a priori* unknown smearing or blocking function  $f_k(\tau k^2)$  which regulates the UV and IR divergent proper-time integration, respectively.

The convergence of the approximate solution of the flow equation is partly controlled by the regulator and can be accelerated if a certain blocking function is chosen. In previous works [9, 10] the regulator was given by

$$f_k^{(i,d)} = \frac{2^i(d-2)!!}{\Gamma(d/2)(d-2+2i)!!} \Gamma(d/2+i, \tau k^2) \quad (5)$$

for  $d = 4$  dimensions. In Refs. [9, 10] details concerning the choice of regulators and the scheme dependence of the proper-time flow equations for the quark-meson model can be found.

This choice has the disadvantage that the generalization to finite temperature results in Matsubara sums which have to be evaluated numerically. For higher smearing functions i.e. for functions with indices  $i > 1$  more and more additional terms in the flow equations are generated at finite  $T$  and  $\mu$  and render the flow equations more complicated. The choice of the same regulator but now for  $i = 1$  and in  $d = 3$  dimensions, produces an analytic RG flow equation in  $T$  as well as in  $\mu$  and is given explicitly by

$$\partial_t f_k^{(i=1,d=3)}(\tau k^2) = -\frac{8}{3\sqrt{\pi}} (\tau k^2)^{5/2} e^{-\tau k^2} . \quad (6)$$

Then only one threshold function for each physical degree of freedom arises and the structure of the full RG flow equation for the thermodynamic potential in the vacuum becomes simple and physically intuitive. Also the finite  $T$  and  $\mu$  generalization is straightforward.

In thermal equilibrium, we apply the Matsubara technique and follow the standard procedure. The quark chemical potential is introduced in the fermionic piece of the Lagrangian by the replacement  $\partial_0 \rightarrow \partial_0 - i\mu$  in the

time-component of the derivative. The finite-temperature extension of this PTRG method is described in detail in Ref. [9] for an  $O(N)$ -model and in Ref. [10] for the quark-meson model.

In the Matsubara formalism, the integration over the zero-component of the momentum is replaced by a summation over Matsubara frequencies,  $\omega_n$ , for mesons and,  $\nu_n$ , for the quarks:

$$\omega_n = 2n\pi T \quad , \quad \nu_n = (2n + 1)\pi T \quad , \quad n \in \mathbb{Z} \quad , \quad (7)$$

such that for an arbitrary function  $g(p)$

$$\int \frac{d^4 p}{(2\pi)^4} g(\vec{p}, p_4) \rightarrow T \sum_{n=-\infty}^{\infty} \int \frac{d^3 p}{(2\pi)^3} g(\vec{p}, \left\{ \begin{array}{c} \nu_n + i\mu \\ \omega_n \end{array} \right\}) \quad (8)$$

for Fermions and Bosons, respectively.

In order to solve the RG equation (3), a truncation of the effective action is necessary. We will use the lowest-order in a derivative expansion of the effective action given in Eq. (1) at a given UV scale  $\Lambda$ . This yields a single partial differential equation for the scale-dependent grand canonical thermodynamic potential  $\Omega(T, \mu; \phi)$  which depends on  $T$ ,  $\mu$  and the fields  $\phi$ :

$$\begin{aligned} \partial_t \Omega_k(T, \mu; \phi) = & -\frac{T}{2} \int_0^\infty \frac{d\tau}{\tau} \left[ \partial_t f_k^{(i=1, d=3)} \right] \sum_n \int \frac{d^3 q}{(2\pi)^3} \text{Tr} \left[ e^{-\tau(\omega_n^2 + \vec{q}^2 + \frac{\partial^2 \Omega_k(T, \mu; \phi)}{\partial \phi_i \partial \phi_j})} \right. \\ & \left. - e^{-\tau[(\nu_n + i\mu)^2 + \vec{q}^2 + g^2 \phi^2]} \right] . \end{aligned} \quad (9)$$

Only the fermionic potential contribution is modified explicitly by the finite quark chemical potential. At this stage, one sees nicely the additive separation of the mesonic and fermionic flow in this approximation. Note, that we use the same blocking function for the bosonic and fermionic flow-equation contributions.

Evaluating the traces and performing the remaining three-momentum integrals, we finally obtain

$$\begin{aligned} \partial_t \Omega_k(T, \mu; \phi) = & -\frac{T}{2(4\pi)^{3/2}} \int_0^\infty \frac{d\tau}{\tau^{5/2}} \left[ \partial_t f_k^{(i=1, d=3)} \right] \\ & \sum_n \left\{ 3e^{-\tau(\omega_n^2 + 2\Omega'_k)} + e^{-\tau(\omega_n^2 + 2\Omega'_k + 4\phi^2 \Omega''_k)} - 4N_c N_f e^{-\tau[(\nu_n + i\mu)^2 + g^2 \phi^2]} \right\} \end{aligned} \quad (10)$$

where the  $\phi$ -dependence of the potential derivatives on the right-hand side has been suppressed. The primed potential denotes the  $\phi^2$ -derivative, *i.e.*  $\Omega'_k := \partial\Omega_k/\partial\phi^2$  etc. In the following, we define the pion-,  $\sigma$ -meson and quark energies as

$$E_\pi = \sqrt{k^2 + 2\Omega'_k}, \quad E_\sigma = \sqrt{k^2 + 2\Omega'_k + 4\phi^2\Omega''_k}, \quad E_q = \sqrt{k^2 + g^2\phi^2}. \quad (11)$$

Evaluating the potential  $\Omega_k$  at the global minimum,  $\phi_0$ , the scale-dependent effective meson masses are defined as  $m_{\sigma,k}^2 = (2\Omega'_k + 4\phi^2\Omega''_k)|_{\phi=\phi_0} = 4\phi_0^2\Omega''_k(\phi_0)$  and  $m_{\pi,k}^2 = 2\Omega'_k|_{\phi=\phi_0} = 0$ . The dynamically generated (constituent) quark masses  $m_{q,k} = g\phi_0$  are proportional to the minimum since we do not consider the running of the Yukawa coupling constant.

Finally, the PTRG flow equation for the scale-dependent grand canonical potential can be integrated analytically, resulting in

$$\begin{aligned} \partial_t\Omega_k(T, \mu; \phi) = & \frac{k^5}{12\pi^2} \left[ \frac{3}{E_\pi} \coth\left(\frac{E_\pi}{2T}\right) + \frac{1}{E_\sigma} \coth\left(\frac{E_\sigma}{2T}\right) \right. \\ & \left. - \frac{2N_c N_f}{E_q} \left\{ \tanh\left(\frac{E_q - \mu}{2T}\right) + \tanh\left(\frac{E_q + \mu}{2T}\right) \right\} \right] \quad (12) \end{aligned}$$

This flow equation is the full RG equation in the approximation considered for finite temperature and chemical potential. Note, that since we have neglected the running of the Yukawa coupling, the approximation does not correspond to the local potential approximation (LPA). It is possible to rewrite Eq. (12) by means of occupation numbers (cf. Ref. [11, 12]).

The different degrees of freedom contribute in an additive way to the flow. One recognizes the three (degenerate) pion-, the sigma- and the quark/anti-quark threshold functions in the square brackets. The flow equation has an overall scale factor  $k^4$ , the correct dimension of the potential in  $d = 4$  dimensions, which can be seen explicitly by rewriting all threshold functions in a dimensionless form. Due to the fermion loops, the fermionic contributions enter with a negative sign and have a degeneracy factor of  $(2s + 1) \times N_c \times N_f$  with  $s = 1/2$ . Only in the quark/anti-quark threshold functions the quark chemical potential enters with the appropriate sign as it should be.

## 2.1 Analytical limits

It is instructive to investigate analytical limits of the full flow equation (12). The flow in the vacuum is given by

$$\partial_t \Omega_k(0, 0; \phi) = \frac{k^5}{12\pi^2} \left[ \frac{3}{E_\pi} + \frac{1}{E_\sigma} - \frac{4N_c N_f}{E_q} \right]. \quad (13)$$

Due to spontaneous chiral symmetry breaking, the quark energies  $E_q$  are always positive and contribute to the flow. In the mesonic threshold functions poles can emerge, depending on the shape of the potential. For instance, the pion pole for  $\phi = 0$  is determined exactly by the condition  $\Omega'_k = -k^2/2$ . However, for an appropriate choice of initial conditions at the UV scale  $\Lambda$ , the poles are never reached during the  $k$ -evolution.

For finite  $T$  but vanishing  $\mu$ , the difference between fermionic and bosonic Matsubara sums in  $\partial_t \Omega_k(T, 0)$  vanishes in the low-temperature limit and we regain the vacuum flow analytically. For finite  $\mu$  and  $T = 0$ , on the other hand, the flow is governed by the non-analytic equation

$$\partial_t \Omega_k(0, \mu; \phi) = \frac{k^5}{12\pi^2} \left[ \frac{3}{E_\pi} + \frac{1}{E_\sigma} - \frac{4N_c N_f}{E_q} \{1 - \theta(\mu - E_q)\} \right] \quad (14)$$

reflecting the existence of the Fermi surface. Thus, in the zero-temperature limit, the tanh-expressions in the fermionic threshold functions of Eq. (12) degenerate to  $2\theta(E_q - \mu)$ . It is also possible to analytically perform the zero chemical-potential limit of Eq. (12) which again yields the correct vacuum flow since the fermionic flow contribution in the curly brackets tends to two.

For hadronic matter in thermal equilibrium, two new energy scales  $T$  and  $\mu$  enter the evolution equation. The quark chemical potential influences the bosonic part  $\partial_t \Omega_k^{\text{Boson}}$  only implicitly through the meson masses. If the bosonic fluctuations are neglected by setting  $\partial_t \Omega_k^{\text{Boson}} = 0$ , one obtains (for a constant Yukawa coupling) standard mean-field theory results for the thermodynamic potential. The remaining quark contribution can then easily be integrated [13]. This feature is also seen in other RG approaches (e.g. in Ref. [14]). As is well known, mean-field theory does not always give a reliable description of the phase transition near criticality as it neglects the role of the important (thermodynamic) fluctuations. We will come back to this point below.

Rewriting the step-function as in Eq. (14), one recognizes easily that the quark flow contribution splits into a vacuum and finite-chemical potential

part with opposite sign. For  $\mu < E_q = g\phi_{0,k=0}$ , the finite- $\mu$  part vanishes and there is no distinction to the vacuum flow. In the vacuum, spontaneous chiral symmetry breaking is mainly driven by the quark fluctuations, while meson fluctuations tend to restore chiral symmetry due to the relative sign in the flow Eq. (12). The relative sign between the vacuum and finite density part in the quark sector of Eq. (14) suppresses the quark fluctuations which are important for chiral symmetry restoration at high densities.

## 2.2 Solving the flow equation

In order to solve the flow Eq. (12) numerically one has in principle two possibilities: either one can discretize the unknown potential  $\Omega_k$  on a  $\phi^2$ -grid or expand the potential in powers of  $\phi^2$  around its minimum  $\phi_0$ . The advantage of a potential expansion is that only a few coupled flow equations have to be solved, depending on the number of couplings in the potential. But for each higher order of the potential expansion, a new coupled beta function arises which increases the numerical effort drastically. A further disadvantage is that the potential, after the evolution, is only known at the (local) minimum  $\phi_0$ .

The big advantage of the grid solution is that one knows the potential not only for the minimum but also for arbitrary  $\phi^2$ . This is of importance for a first-order phase transition where two degenerate minima of the potential emerge. In order to describe the first-order transition correctly, the knowledge of all local minima is required. This is cumbersome in a potential expansion, except for some simple potentials. For finite pion masses, i.e. with an additional explicit symmetry breaking term in the potential, every minimum has always a finite value and the symmetry is never exactly restored. Also in this case, a precise determination of the critical temperature of a first-order transition is very difficult within an expansion scheme around only one minimum. The solution on a grid is, however, computationally very demanding since one encounters highly-coupled and rather large matrix equations in order to obtain reliable accuracy. Nonetheless, for the reasons given above, we opted for the grid solution but will also compare the findings with results from a potential expansion.

In order to solve the flow equation (12), we discretize the field  $\phi^2$  for a general potential term on a regular grid. Details of the algorithm which has been adapted to include fermions, can be found in Ref. [9] and references therein. The task is then to solve the resulting closed coupled set of flow



equations for the potential by starting the evolution in the ultraviolet and integrate towards  $k = 0$  for each grid point. In this limit, all quantum- and thermal fluctuations are taken into account. It turns out that the numerical convergence is faster if one works with the dimensionful flow equation instead of the rescaled one. The initial conditions are chosen at the UV scale  $\Lambda$  in such a way that they match physical vacuum quantities obtained in the IR. Predictions for finite temperature and density are then possible without any further parameter adjustments. As initial condition we use the tree-level parameterization of the symmetric potential

$$V_\Lambda(\phi^2) = \frac{\lambda}{4}(\phi^2)^2 - \frac{\lambda}{2}\phi_0^2\phi^2 \Big|_\Lambda \quad (15)$$

at the compositeness scale  $\Lambda = k_{\chi_{SB}}$ . For the results presented below we choose  $\Lambda = 500$  MeV,  $\lambda = 10$  and  $\phi_0^2 = 0$ . The number of grid points is typically chosen around 60 – 100 for a  $\phi$ -interval between 0 and 100. We have tested, that the numerical results do not change by varying the number of grid points. The precise value of  $\phi_0^2$  is not important, since it has little influence on the vacuum results in the infrared where chiral symmetry is spontaneously broken. The Yukawa coupling is fixed to  $g = 3.2$  in order to reproduce a constituent quark mass of the order of 300 MeV. These choices of initial parameters yield a vacuum pion decay constant of  $f_\pi \sim 87$  MeV in the chiral limit which is consistent with values obtained from chiral perturbation theory [15] and previous works [9]. For finite and realistic pion masses, this value is shifted to  $f_\pi \sim 93$  MeV.

### 3 The phase diagram for $N_f = 2$

Recently, significant progress has been made in studies of the QCD thermodynamics with chemical potential by numerical simulations of lattice gauge theory. Different methods of extrapolation to the finite- $\mu$  region are in reasonable agreement [17, 18, 19] concerning the pseudocritical line  $T_c(\mu)$  out to chemical potential values of several 100 MeV [20, 21, 22]. This allows for a direct comparison of lattice simulations with our nonperturbative method. Some recent results of the leading non-trivial term of quadratic order in the Taylor expansion of the pseudocritical line are listed in Tab. 1 and compared to the one obtained with the PTRG method.

	$T_c \left. \frac{d^2 T_c}{d\mu^2} \right _{\mu=0}$
PTRG (full)	-0.23
PTRG ( $\phi^4$ )	-0.258
Lattice (Taylor)	-0.14(6)
Lattice ( $\mu_I$ )	-0.101
NJL (mean-field)	-0.4

Table 1: The curvature of the  $N_f = 2$  transition line for small quark chemical potentials compared with different methods.

The curvature of the RG without any truncation, labeled by PTRG (full), is smaller compared to a  $\phi^4$  truncation of the potential within the same RG approach, denoted by PTRG ( $\phi^4$ ). At the expected tricritical point, a first-order phase transition emerges where higher monomials in the potential expansion will become necessary. On the other hand, we know that the truncation works well for the finite temperature and zero chemical potential phase transition. It turns out that the  $\phi^4$  truncation breaks down at finite quark chemical potentials around  $\mu \sim 100$  MeV [23].

Note that the RG results are obtained for zero quark masses in contrast to the lattice simulations (see e.g. table 1 in Ref. [16] for recent lattice pion masses in physical units). On the lattice (e.g. Ref. [17]), realistic light quark masses have not yet been achieved in a Taylor series estimate of the reweighting factor up to quadratic order in  $\mu$ . The first Taylor coefficient corresponds to the curvature and is labeled by (Taylor) in the Table. The equivalent coefficient obtained with the imaginary chemical potential method is denoted by ( $\mu_i$ ) in the Table [18]. However, the lattice results of Ref. [17] suggest that any dependencies of the curvature on the quark masses are weak. Compared to the chiral limit we see a difference of a factor two. A mean-field calculation within a NJL-model in the chiral limit yields the largest curvature. However, the curvature depends strongly on the chosen parameter set for the NJL model [24].

In Fig. 1 we show the chiral phase diagram for the two flavor linear quark-meson model in the chiral limit. At  $\mu = 0$ , a second-order phase transition with a critical temperature of  $T_c \sim 142$  MeV is found in which

the spontaneously broken chiral symmetry is restored. Note that the critical temperature is not a universal quantity and depends on the fitted pion decay constant in the vacuum. The phase transition and fixed point structure is in the  $O(4)$  universality class and was investigated within the same PTRG framework in detail in Ref. [9].

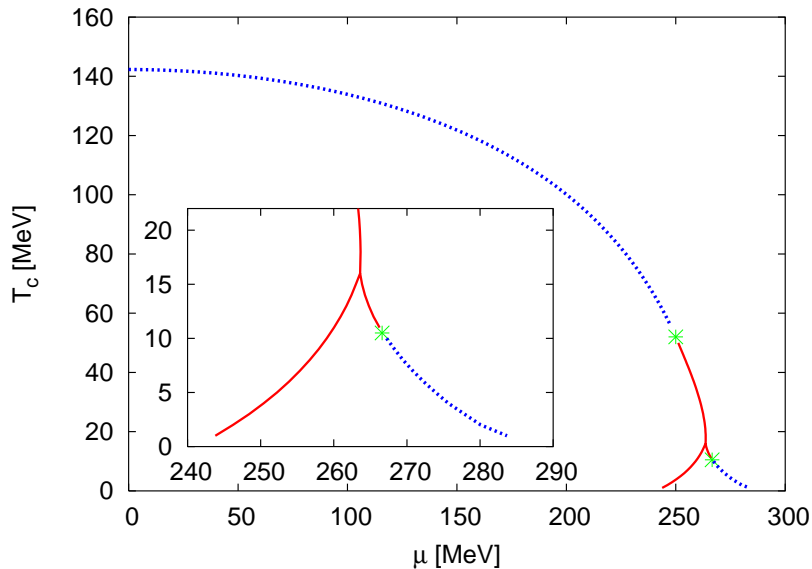


Figure 1: The phase diagram of the two-flavor quark-meson model in the chiral limit. The tricritical points are denoted by an asterisk. For  $\mu$  below the upper tricritical point the transition is of second-order (dashed line) and belongs to the  $O(4)$  universality class. For temperatures smaller than  $T < 17$  MeV the single first-order phase transition (solid line) splits into two phase transitions. The left transition line is always of first-order while the chiral restoration transition line around the splitting point is initially of first-order (solid line) and turns into a second-order (dashed line) phase transition for smaller temperatures.

For realistic pion masses the second-order phase transition is washed out and becomes a smooth crossover. This results in a larger “critical” temperature of the order of 180 MeV [25].

For finite chemical potential, the second-order phase transition with  $O(4)$  critical exponents persists up to a tricritical point. The location of this tricritical point is found to be at  $T_{c,tri} = 52$  MeV and  $\mu_{c,tri} = 251$  MeV for the

initial conditions chosen. Within a nonperturbative expansion scheme, similar results are found in Ref. [26]. This point belongs to a trivial Gaussian fixed point with mean-field critical exponents as we have verified explicitly [27].

For finite (realistic) pion masses, model calculations and lattice simulations suggest a range of  $T \sim 100 - 180$  MeV and  $\mu_B \sim 50 - 700$  MeV for the location of the critical point of QCD [2]. The critical mean-field region of the endpoint, where the mean-field theory of phase transitions is still valid, is further expected to be small [3]. Nevertheless, the qualitative features of the phase diagram which we address, do not depend on the chosen initial conditions. Thus, the existence of this point, the shape of the transition lines and its universality class is a prediction within the underlying model.

At higher chemical potentials and smaller temperatures, the phase transition changes initially to a single first-order phase transition. For critical temperatures below  $T_s \sim 17$  MeV and around  $\mu_s \sim 263$  MeV, however, we observe a splitting of the transition line and two phase transitions emerge. The left transition line (see magnified panel in Fig. 1) represents a first-order transition down to the  $T = 0$ -axis. At this transition, the order parameter jumps not to zero but to a finite value (Fig. 2). The chiral symmetry remains spontaneously broken and is only restored for higher chemical potentials which produce the second (right) transition line. For temperatures just below the splitting point, i.e. for  $T < 17$  MeV, at the right transition line we initially find a second first-order transition where the order parameter again jumps to zero and chiral symmetry gets restored. But for smaller temperatures close to the  $\mu$ -axis the order parameter tends smoothly to zero. Due to a finite grid spacing it is difficult for such small temperatures to determine the precise order of the transition. It seems, however, that it is again of second-order. The determination of the corresponding universality class is postponed to future work [23]. Nevertheless, we infer that there must be a second tricritical point in the phase diagram.

In Fig. 2 the order parameter, which corresponds to the expectation value (VEV) of the  $\sigma$ -field, is shown as function of the chemical potential for three different temperatures in the splitting area of the phase diagram (Fig. 1). Around the splitting point at  $T = 15$  MeV, the order parameter depends slightly on the chemical potential  $\mu$  before the first transition, thus washing out the edge at the gap. The  $\mu$ -dependence becomes weaker for decreasing temperatures. For  $T = 1$  MeV there is almost no difference between the finite-density and vacuum evolution and the order parameter stays at the vacuum value  $\phi \sim 87$  MeV. For  $T = 15$  MeV two gaps in the order parameter

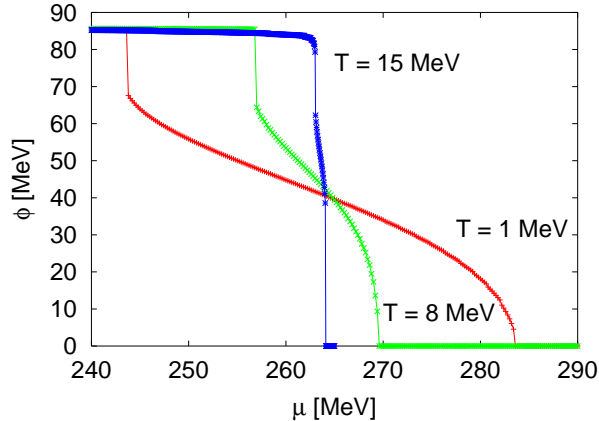


Figure 2: The order parameter  $\phi$  versus chemical potential for three different temperatures.

corresponding to two phase transitions can be seen. The magnitude of the first gap is almost constant and independent of the temperature. For smaller temperatures ( $T < 8$  MeV), the VEV as a function of  $\mu$ , smoothly decreases to zero after the first transition and stays zero for larger chemical potentials. This is a signal that the system undergoes a second-order transition again. Finally, chiral symmetry is completely restored. It is interesting to observe that all curves intersect roughly at the same critical chemical potential of the splitting point,  $\mu_s$ , where the magnitude of the VEV is about one half of the vacuum value.

The exact location of the splitting point and the first-order gap of the order parameter depends on the chosen vacuum quark masses. For larger vacuum quark masses e.g. of the order of 380 MeV, corresponding to a larger Yukawa-coupling of 4.2, the location of the splitting point moves down to smaller temperatures and larger chemical potentials. The gap in the order parameter of the first-order transition increases with the quark masses. Thus, varying the vacuum quark masses within say 250 – 450 MeV, the area bounded by the transition lines is reduced. Yet, the order of the phase transition lines are not altered.

It is also instructive to see both phase transitions in the thermodynamic potential explicitly. In Fig. 3 the  $k$ -evolution below the splitting point is shown for  $T = 9$  MeV and  $\mu = 254$  MeV for different (small) IR scales. The

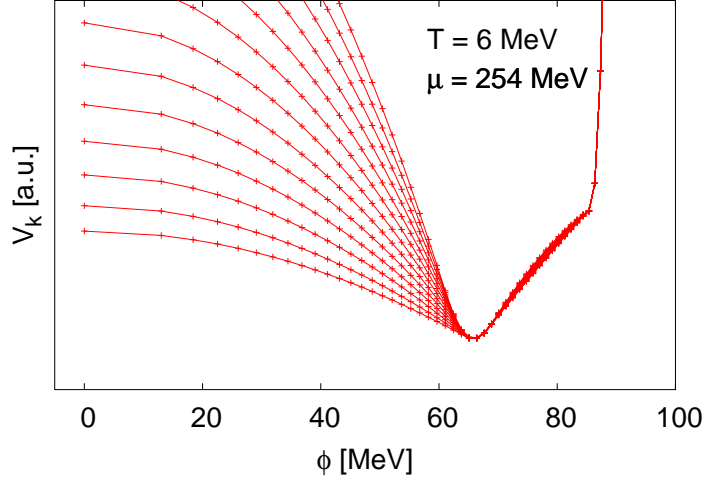


Figure 3: The scale evolution of the thermodynamic potential towards the infrared is shown as a function of the field  $\phi$  below the splitting point for  $T = 6$  MeV and  $\mu = 254$  MeV. (Lowest line  $k = 8$  MeV,  $\Delta k = 1$  MeV between each line). Since the chemical potential is larger than the critical one, both minima of the potential (one at  $\phi \sim 65$  MeV and the other one at  $\phi \sim 87$  MeV) are no longer equal.

potential exhibits two finite minima.<sup>2</sup> This situation is definitely different compared to that in Fig. 4. Here the scale evolution of a typical second- or first-order transition is shown in the left- and right panel, respectively. For a second-order phase transition we have only one (global) minimum. In the IR, the potential becomes flat (constant) below the minimum and is almost scale independent above. The scale evolution barely effects the minimum. For the chosen initial conditions, this situation is encountered for chemical potentials below 250 MeV and temperatures between 142 - 52 MeV. A typical first-order transition is shown in the right panel of Fig. 4 near the critical point. Here, a second minimum at the origin emerges and the global minimum jumps to zero for larger chemical potentials. In all cases, the potential tends to a convex function but the scale evolution of the nontrivial minimum is very weak. This justifies to terminate the numerical evolution at a finite but small

<sup>2</sup>For any finite IR scale (which is numerically always realized) the potential is not exactly convex. Only in the IR limit  $k = 0$ , it becomes convex as can be seen in the Fig. 4 [28].

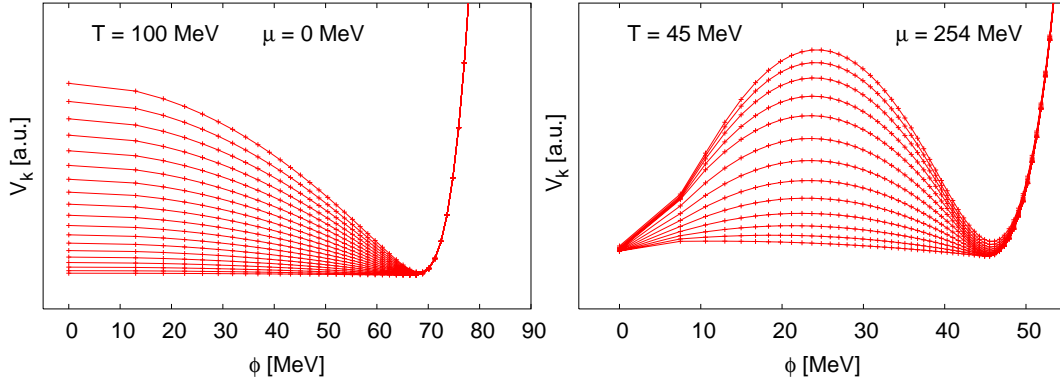


Figure 4: Typical scale evolution towards the infrared of a second-order phase transition (left panel) and first-order transition (right panel). (Lowest line  $k = 2$  MeV,  $\Delta k = 1$  MeV between each line. See text for further details).

IR scale (typically  $k < 1 - 10$  MeV) [28].

The pressure  $p(T, \mu) = -\Omega_{k=0}(T, \mu, \phi_0)$  evaluated at the global minimum  $\phi_0$  is normalized to zero in the vacuum. For finite chemical potential and vanishing temperature, it stays strictly zero up to the transition point. Therefore, the quark number density,  $n_q = \partial p / \partial \mu$ , jumps to a finite value. Afterwards it increases monotonically. Quantitatively, the quark number density jumps to  $0.1 \text{ fm}^{-3}$  at  $\mu \sim 242$  MeV which corresponds to a normalized baryon density  $\rho_B / \rho_0 \sim 0.18$ . These values are obtained for a vacuum quark mass of  $\sim 275$  MeV and increase significantly towards more realistic values if the vacuum quark mass is increased. These observations strongly suggest that the system undergoes a gas-liquid transition to bound quark matter, where the chiral symmetry remains spontaneously broken. Thus, the “triangular region” in Fig. 1 consists of a bound mixture of massive quarks/antiquarks, interacting massless pions and massive sigma mesons.

## 4 Conclusions

In order to provide a reliable identification of the phase structure of strongly interacting matter, one must invoke nonperturbative methods such as the Wilsonian formulation of the renormalization group. We have employed a self-consistent RG approach with a smooth proper-time regularization. As

an effective realization of QCD for two flavors, a linear quark-meson model has been used with an arbitrary  $O(4)$ -symmetric mesonic potential term. To explore the phase diagram in the  $(T, \mu)$ -plane we have extended previous studies to finite temperature and quark chemical potential. The resulting RG equations for the potential term have been solved numerically in the chiral limit. The first non-trivial coefficient of the transition line which belongs to the  $O(4)$  universality class, has been determined and compared with recent lattice simulations. The curvature in the chiral limit is larger by a factor two as compared to lattice analyses. The latter, however, employ unrealistically large  $u - d$  current quark masses.

The location of the tricritical point, governed by a Gaussian fixed point, has been determined. This structure of the phase diagram is similar to the results of other works, where the second-order transition line ends in a tricritical point and turns into a single phase transition of (weak) first-order for decreasing temperatures [27, 26]. This first-order transition persists up to zero temperature and finite chemical potential.

For  $\mu > \mu_c$  we also find initially a first-order transition which splits into two phase transitions for temperatures below 17 MeV. The left transition line is always of first-order. The value for the splitting point depends on the initial condition for dynamically generated constituent quark mass in the vacuum. Apart from the dependencies on the initial conditions, further uncertainties arise from the truncation scheme of the flow equation which may affect the exact values of the critical temperature and chemical potential. It is difficult to obtain quantitative error estimates in this context. The main focus of this work is not a quantitative prediction of some non-universal numbers but the qualitative feature of the phase diagram of the two-flavor linear quark-meson model.

For larger quark masses the splitting point moves towards smaller temperatures but all qualitative features of the transition lines persist. Along the chiral symmetry restoration line below the splitting point, the transition is initially also of first-order but then turns into a second-order transition. This leads to the suggestion that the QCD phase diagram may have a second “tricritical” point.

The triangular region in the phase diagram which is a new feature of our calculation, is not related to spinodal curves or metastable phases. It is an effect driven by fluctuations. In a mean-field calculation, we only find one single first-order transition in which chiral symmetry is restored (see also [29]). The full RG treatment, however, renders the order parameter and



hence the constituent quark mass finite beyond the first-order transition line. At the transition the quark-number density jumps from zero to a finite value and increases monotonically with increasing  $\mu$ . We interpret this transition as the liquid-gas transition to a state of bound quark matter, consisting of interacting constituent quarks.

There are several directions in which the present analysis should be extended. A obvious one is to include explicit chiral symmetry breaking via finite current quark masses [23]. This will turn the second-order transitions into smooth cross overs. From lattice studies it is well known that the strange quarks mass plays a decisive role in the location of the critical endpoint. For infinitely heavy strange quarks, in fact, it lies at  $\mu = 0$ ! Thus, it is mandatory to extend our calculations to  $N_f = 3$ . While this is a computational challenge it will provide more realistic results. Work in this direction is in progress.

## Acknowledgments

We would like to thank Michael Buballa for useful and illuminating discussions. This work was supported in part by BMBF grant 06 DA 116.

## References

- [1] R.D. Pisarski and F. Wilczek, Phys. Rev. **D29** (1984) 338.
- [2] M.A. Stephanov, hep-ph/0402115v1; D.T. Son and M.A. Stephanov, hep-ph/0401052v1.
- [3] Y. Hatta and T. Ikeda, Phys. Rev. **D67** (2003) 014028.
- [4] K. Rajagopal and F. Wilczek, Chapter 35 in the Festschrift in honor of B. L. Ioffe, "At the Frontier of Particle Physics / Handbook of QCD", M. Shifman, ed., (World Scientific) hep-ph/0011333.
- [5] M. Oleszczuk, Z. Phys. **C64** (1994) 533; S.-B. Liao, Phys. Rev. **D53** (1996) 2020; S.-B. Liao, Phys. Rev. **D56** (1997) 5008.
- [6] D. Zappalà, Phys. Rev. **D66** (2002) 105020; P. Castorina et al., Phys. Lett. **B567** (2003) 31.

- [7] D.F. Litim and J.M. Pawłowski, Phys. Lett. **B546** (2002) 279 and References therein.
- [8] D.F. Litim and J.M. Pawłowski, Phys. Rev. **D66** (2002) 025030.
- [9] O. Bohr, B.-J. Schaefer, J. Wambach, Int. J. Mod. Phys. **16** (2001) 3823.
- [10] G. Papp, B.-J. Schaefer, H.-J. Pirner, J. Wambach, Phys. Rev. **D61** (2000) 096002.
- [11] J. Braun, K. Schwenzer and H.-J. Pirner, hep-ph/0312277.
- [12] J. Meyer, G. Papp, H.-J. Pirner and T. Kunihiro, Phys. Rev. **C61** (2000) 035202.
- [13] O. Scavenius, A. Mocsy, I.N. Mishustin and D.H. Rischke, Phys. Rev. **C64** (2001) 045202.
- [14] C. Bagnuls and C. Bervillier, Phys. Rept. **348** (2001) 91; J. Berges, N. Tetradis and Ch. Wetterich, Phys. Rept. **363** (2002) 223.
- [15] P. Gerber and H. Leutwyler, Nucl. Phys. **B321** (1989) 387; J. Gasser and H. Leutwyler, Nucl. Phys. **B250** (1985) 517.
- [16] K.-I. Ishikawa, hep-lat/0410050.
- [17] C.R. Allton et al., Phys. Rev. **D66** (2002) 074507; hep-lat/0305007.
- [18] Ph. de Forcrand and O. Philipsen, Nucl. Phys. **B642** (2002) 290.
- [19] Z. Fodor and S.D. Katz, Phys. Lett. **B534** (2002) 87; hep-lat/0104001; hep-lat/0402006.
- [20] S.D. Katz, hep-lat/0310051.
- [21] F. Karsch and E. Laermann, hep-lat/0305025v1.
- [22] F. Karsch, in Proceedings “Lectures on Quark Matter”, Graz 2001.
- [23] B.-J. Schaefer and J. Wambach, work in progress.
- [24] M. Buballa, Phys. Rept. **407** (2005) 205.

- [25] B.-J. Schaefer and H.-J. Pirner, Nucl. Phys. **A660** (1999) 439.
- [26] A. Jakovac, A. Patkos, Zs. Szep and P. Szepfalusy, hep-ph/0312088.
- [27] N. Tetradis, Nucl. Phys. **A726** (2003) 93; N. Brouzakis and N. Tetradis, hep-th/0401074v1.
- [28] A. Bonanno and G. Lacagnina, Nucl. Phys. **B693** (2004) 36.
- [29] M. Buballa, Nucl. Phys. **A611** (1996) 393.